

Bryan Mackenzie · M. L. Ujwal · Min-Hwang Chang
Michael F. Romero · Matthias A. Hediger

Divalent metal-ion transporter DMT1 mediates both H⁺-coupled Fe²⁺ transport and uncoupled fluxes

Received: 8 June 2005 / Accepted: 7 July 2005 / Published online: 10 August 2005
© Springer-Verlag 2005

Abstract The H⁺-coupled divalent metal-ion transporter DMT1 serves as both the primary entry point for iron into the body (intestinal brush-border uptake) and the route by which transferrin-associated iron is mobilized from endosomes to cytosol in erythroid precursors and other cells. Elucidating the molecular mechanisms of DMT1 will therefore increase our understanding of iron metabolism and the etiology of iron overload disorders. We expressed wild type and mutant DMT1 in *Xenopus* oocytes and monitored metal-ion uptake, currents and intracellular pH. DMT1 was activated in the presence of an inwardly directed H⁺ electrochemical gradient. At low extracellular pH (pH_o), H⁺ binding preceded binding of Fe²⁺ and its simultaneous translocation. However, DMT1 did not behave like a typical ion-coupled transporter at higher pH_o, and at pH_o 7.4 we observed Fe²⁺ transport that was not associated with H⁺ influx. His²⁷² → Ala substitution uncoupled the

Fe²⁺ and H⁺ fluxes. At low pH_o, H272A mediated H⁺ uniport that was inhibited by Fe²⁺. Meanwhile H272A-mediated Fe²⁺ transport was independent of pH_o. Our data indicate (i) that H⁺ coupling in DMT1 serves to increase affinity for Fe²⁺ and provide a thermodynamic driving force for Fe²⁺ transport and (ii) that His-272 is critical in transducing the effects of H⁺ coupling. Notably, our data also indicate that DMT1 can mediate facilitative Fe²⁺ transport in the absence of a H⁺ gradient. Since plasma membrane expression of DMT1 is upregulated in liver of hemochromatosis patients, this H⁺-uncoupled facilitative Fe²⁺ transport via DMT1 can account for the uptake of nontransferrin-bound plasma iron characteristic of iron overload disorders.

Keywords Iron transport · Metal-ion transport · Proton-coupled transport · Cotransporters · Zinc transport · Oocyte · *Xenopus laevis* · Iron overload

B. Mackenzie · M. L. Ujwal · M. A. Hediger
Membrane Biology Program and Renal Division,
Brigham and Women's Hospital and Harvard Medical School,
77 Avenue Louis Pasteur, Boston, MA 02115, USA

M.-H. Chang · M. F. Romero
Department of Physiology and Biophysics, Case Western Reserve
University School of Medicine, 2119 Abington Road, Cleveland,
OH 44106-4970, USA

M. F. Romero
Department of Pharmacology, Case Western Reserve University
School of Medicine, 2119 Abington Road, Cleveland,
OH 44106-4970, USA

B. Mackenzie
Department of Molecular and Cellular Physiology,
University of Cincinnati College of Medicine,
P.O. Box 670576, Cincinnati, OH 45267-0576, USA

M. A. Hediger (✉)
Institute for Biochemistry and Molecular Biology,
University of Berne, Bühlstrasse 28,
CH-3012 Bern, Switzerland
E-mail: matthias.hediger@mci.unibe.ch
Tel.: +41-31-6314129
Fax: +41-31-6313410

Introduction

The DMT1 is a widely expressed, mammalian ferrous-iron (Fe²⁺) transporter that is energized by the H⁺ electrochemical potential gradient [19, 33]. Its importance as a principal mechanism of intestinal Fe²⁺ absorption and erythroid iron utilization is highlighted by the severe microcytic anemia characteristic of the *mk* mouse and Belgrade (*b*) rat, inbred rodent strains that bear an identical (G185R) mutation in DMT1 [12, 13, 16]. Analyses of DMT1 mRNA and protein distribution, as well as metal-ion transport assays in isolated cells, cell lines, or in vivo, suggest that DMT1 mediates not only apical iron uptake in the intestine and kidney [4, 5, 53, 56], but also the recovery of iron from recycling endosomes during transferrin receptor (TfR)-associated cellular uptake in erythroid precursor cells and most other cell types [5, 12, 15, 45].

In the small intestine, DMT1 mRNA and protein are expressed in enterocytes throughout the small intestine,

most strongly in the proximal duodenum, where the expression of DMT1 is tightly regulated by body iron status [5, 19, 23]. The acidic microclimate of the intestinal brush border [37] is thought to drive H^+ -coupled Fe^{2+} uptake via DMT1 into enterocytes. In erythroid cells, DMT1 colocalizes with transferrin and TfR in recycling endosomes [6, 18, 50, 52]. Acidification of the endosomal lumen by the V-type H^+ -ATPase [52] permits the dissociation of Fe^{3+} from transferrin, accelerates its reduction to Fe^{2+} [41], and provides the H^+ gradient to energize DMT1-mediated Fe^{2+} transport from endosome to cytosol.

When expressed in *Xenopus* oocytes, rat DMT1 exhibited moderately high apparent affinity for Fe^{2+} and several other transition metal ions [19]. The Fe^{2+} transport was voltage-dependent and H^+ -coupled [19]. Cotransport with H^+ was also demonstrated in the intestinal Caco-2 cell line [51], which is known to express DMT1 [2, 51]. In the present study—using the two-microelectrode voltage clamp, radiotracer uptake assays, and intracellular pH-sensing microelectrodes—we have performed a kinetic analysis of DMT1 and present a model that describes H^+ and Fe^{2+} transport mediated by DMT1. Analysis of the impact of mutations at two histidyl residues residing within transmembrane region 6 (TM6) both supports our model for DMT1 and constitutes an important step in structure-function analysis of this transport protein. Elucidating the molecular mechanisms of DMT1 will lead to a better understanding of the contribution of DMT1 to iron metabolism and the etiology of iron overload disorders.

Methods

Site-directed mutagenesis of rat DMT1

Rat wild type DMT1 (wtDMT1) is the product of the *Slc11a2* gene (and is also known as DCT1 or Nramp2). The wtDMT1 cDNA sequence [19] was excised from pSPORT1 between *SalI* (in the multiple cloning region) and *EcoRI* (at base pair 2111 of the DMT1 cDNA sequence), then subcloned into pBluescript II KS(+) to generate a construct (pBSKmrDMT1) for site-directed mutagenesis. Mutants were generated by PCR amplification of wtDMT1 using sense primers (Table 1)

designed to introduce single amino-acid substitutions at His-267 and His-272. The sense primers also spanned a unique, native *BclI* restriction site (T|GATCA) at base pair 892 of the DMT1 cDNA. Included in each PCR reaction was an antisense primer (5'-ATAGCA GCATGCTATTTGACAAAGACAG-3') identical to wtDMT1 cDNA and which contained a unique, native *SphI* restriction site (GCATG|C, *underlined*) at base pair 1988 of the DMT1 cDNA. The PCR products were gel-purified, double-digested with *BclI* and *SphI*, and ligated into pBSKmrDMT1 between the *BclI* and *SphI* sites. Competent DH5 α cells (Invitrogen) were electrotransformed with the mutant plasmids and selected on LB/agar plates containing 100–200 $\mu\text{g}\mu\text{l}^{-1}$ ampicillin. To restore the 3'-UTR and poly(A) tail and maximize expression in oocytes, the mutated DMT1 sequences were subcloned back into pSPORT1-DMT1. To do so, pSPORT1-DMT1 was first digested with *SmaI* and *Acc65I*, Klenow end-filled and re-ligated, thus removing the *SmaI*-to-*KpnI* fragment (containing an *EcoRI* site) of the multiple cloning region. A clone with only a single *EcoRI* restriction site (within the DMT1 3'-UTR) was selected. Meanwhile, mutant DMT1 sequences were excised from pBSKmrDMT1 between *SalI* and *EcoRI* of the multiple cloning region and ligated into the modified pSPORT1-DMT1 between the *SalI* and *EcoRI* sites (swapping out the wild type sequence). The DH5 α cells were electrotransformed with the modified pSPORT1 containing mutant DMT1 sequences and selected on LB/agar-ampicillin plates as before. Mutations at His-267 and His-272 were verified by DNA sequencing of the final constructs (at the Sequencing Facility of Beth Israel Deaconess Medical Center, Boston, MA, USA) using the sense primer 5'-ATC CTGTTTCAGGCTGCCA-CACCCC-3' (base pairs 833–856 of the DMT1 sequence) and the antisense primer 5'-GGTCA GCATGGGGGCTGCTGC-3' (base pairs 1134–1114).

Expression of wild type and mutant rat DMT1 in *Xenopus* oocytes

The pSPORT1 vector containing wild type or mutant rat DMT1 under the T7 promoter was linearized with *NotI*. The cRNA was synthesized in vitro with the use of the mMESSAGE mMACHINE kit (Ambion) with T7 RNA

Table 1 Oligonucleotide sense primers used for site-directed mutagenesis of rat DMT1

Mutation	Oligonucleotide primer sequence
H267A	5'-GAGCTG TGATCATGCCAGCTAACATGTACCTGCACTCTGCC-3'
H267D	5'-GGGAGCTG TGATCATGCCAGATAACATGTACCTGCACTCTGCC-3'
H267N	5'-GGGAGCTG TGATCATGCCAAACAACATGTACCTGCACTCTGCC-3'
H272A	5'-GAGCTG TGATCATGCCACACAACATGTACCTGGCTTCTGCC-3'
H272R	5'-GGGAGCTG TGATCATGCCACACAACATGTACCTGAGATCTGCCTTAGTC-3'

Sense primers flanked a unique, native *BclI* restriction site (T|GATCA, *underlined*) in the wtDMT1 cDNA sequence and the mutated triplet is shown in boldface. The antisense primer used in each PCR reaction was identical to a fragment of the wtDMT1 nucleotide sequence and contained a unique, native *SphI* restriction site (see text)

polymerase. We performed laparotomy and ovariectomy on adult female *Xenopus laevis* frogs under 2-aminoethylbenzoate anesthesia (0.1% in 1:1 water/ice, by immersion), in compliance with the Harvard Medical Area Standing Committee on Animals. Ovarian tissue was isolated and treated with collagenase A (Roche Diagnostics), and oocytes were isolated and stored at 18°C in modified Barths' medium [32]. Oocytes were injected with ≈50 ng of cRNA and incubated 3–5 days before functional assays were performed.

Media used for transport assays in oocytes

Functional assays in control oocytes and oocytes expressing wild type or mutant rat DMT1 were performed using low-calcium transport media containing L-ascorbic acid (to maintain the iron in its reduced form, Fe^{2+}) and buffered using either (i) MES, HEPES and Tris base, or (ii) MES and piperazine-1,4-bis(2-propanesulfonic acid) (PIPES) as indicated. PIPES, obtained from GFS Chemicals, is a non-complexing buffer with $pK_{a2}^m \approx 8.0$ [60], whereas the commonly used buffers Tris and HEPES are known to complex metal ions [1, 11, 60].

Transport media comprised 100 mM NaCl, 1 mM KCl, 0.6 mM CaCl_2 , 1 mM MgCl_2 , 100 μM L-ascorbic acid (or 1 mM L-ascorbic acid for radiotracer experiments), 0–5 mM MES, and either (i) 0–5 mM PIPES and 0–6 mM NaOH, or (ii) 0–5 mM HEPES and 0–5 mM Tris base. To prepare transport media in the pH range 5.2–7.0, a low-pH medium buffered with 5 mM MES was mixed with appropriate volumes of pH 7.5 media containing either (i) 5 mM PIPES, adjusted to pH 7.5 with NaOH, or (ii) 5 mM HEPES, adjusted to pH 7.5 with Tris base. All experiments were performed at ambient temperature (21–24°C) except where noted (Figs. 1, 6g).

Voltage-clamp experiments

A two-microelectrode voltage clamp (Dagan CA-1B) was used to measure currents associated with wild type or mutant DMT1 in oocytes. Microelectrodes (resistance 0.5–5 M Ω) were filled with 3 M KCl. Voltage-clamp experiments comprised four protocols: (i) Continuous current recordings were made at holding potentials (V_h) of –50 mV, or –70 mV, low-pass filtered at 1 Hz, and digitized at 10 Hz (except for pH_i experiments, see below). (ii) Oocytes were clamped at $V_h = -50$ mV, and step-changes in membrane potential (V_m) were applied from +50 to –150 mV (in 20 mV increments) each for a duration of 200 ms, before and after the addition of Fe^{2+} . Current was low-pass filtered at 500 Hz and digitized at 5 kHz. Steady-state data were obtained by averaging the points over the final 16.7 ms at each V_m step. (iii) Presteady-state currents were obtained at 23 or 28°C using protocol ii modified such that step-changes

were applied from +90 to –130 mV. (iv) Oocytes were clamped at $V_h = -50$ mV, stepped to –150 mV for 13.6 ms (to allow for settling of the capacitive transient currents), and a 1 s ramp applied from –150 to +50 mV. Current was low-pass filtered at 500 Hz and digitized at 5 kHz. Steady-state data from protocols i or ii were fit to a modified 3-parameter Hill relationship (Eq. 1) for which I is the evoked current, I_{\max} the derived current maximum, S the concentration of substrate S (H^+ or metal ion), $K_{0.5}^S$ the substrate concentration at which current was half-maximal, and n_H the Hill coefficient for S .

$$I = \frac{I_{\max} S^{n_H}}{(K_{0.5}^S)^{n_H} + S^{n_H}} \quad (1)$$

To account for the putative H^+ -uncoupled, facilitative Fe^{2+} transport activity (i^U), two alternative functions were tested. In the first, a 4-parameter Hill function (Eq. 2), i^U is a static term (i.e. it does not vary with $[\text{H}^+]_o$) describing the y -intercept, the Fe^{2+} -evoked current at nominally zero H^+ concentration. In the second alternative function (Eq. 3), i^U is not fixed, since increasing $[\text{H}^+]_o$ is assumed to inhibit i^U in favor of $\text{H}^+/\text{Fe}^{2+}$ cotransport. We modified i^U by an exponential decay, the most empirical way of expressing inhibition by H^+ . The $[\text{H}^+]_o$ at which i^U is inhibited 50% is expressed as $\ln(0.5)/-b$.

$$I = i^U + \frac{I_{\max} S^{n_H}}{(K_{0.5}^S)^{n_H} + S^{n_H}} \quad (2)$$

$$I = i^U \exp^{-bS} + \frac{I_{\max} S^{n_H}}{(K_{0.5}^S)^{n_H} + S^{n_H}} \quad (3)$$

Currents obtained over the temperature range 18–31°C (Fig. 6g) were fit with an integrated Arrhenius function (Eq. 4), for which E_a is the Arrhenius activation energy, $\ln A$ the y -intercept, R the universal gas constant (1.987 cal mol $^{-1}$ K), T the absolute temperature, and I the current induced by switching from pH 7.5 to 5.7 ($I^{\text{A pH}}$) or the 50 μM Fe^{2+} -evoked current at pH 5.7 (I^{Fe}).

$$\ln(-I) = \ln A - \frac{E_a}{RT} \quad (4)$$

Following step-changes in V_m using protocol iii, we obtained presteady-state currents in oocytes expressing wild type or mutant DMT1. These were isolated from capacitive transient currents (which decayed with half times of 0.5–0.8 ms) and steady-state currents by the fitted method [21, 32]. Briefly, the first ten points after reaching maximal decay rate were fit using an exponential decay to describe the capacitive transients; these and the final steady-state currents were subtracted to obtain the compensated currents. The compensated currents were integrated with time to obtain charge movement (Q) and fit using the Boltzmann relationship (Eq. 5) for which maximal charge $Q_{\max} = Q_{\text{dep}} - Q_{\text{hyp}}$

(where Q_{dep} and Q_{hyp} represent the charge at depolarizing and hyperpolarizing limits), $V_{0.5}$ is the V_m at the midpoint of charge transfer, z is the apparent valence of the movable charge, and F , R , and T have their usual thermodynamic meanings.

$$\frac{Q - Q_{\text{hyp}}}{Q_{\text{max}}} = \frac{1}{1 + \exp(z[V_m - V_{0.5}]F/RT)} \quad (5)$$

Transporter-mediated presteady-state currents can be used to estimate transporter density [61]. We estimated the number of functional wild type or mutant DMT1 transporters (N_T) per oocyte using Eq. 6, in which e is the elementary charge (1.6×10^{-19} C).

$$N_T = \frac{Q_{\text{max}}}{ze} \quad (6)$$

Radiotracer iron and zinc uptake

We obtained radiochemicals from Perkin-Elmer Life Science Products. The $^{55}\text{Fe}^{2+}$ was used at specific activity 658 MBq mg^{-1} and $^{65}\text{Zn}^{2+}$ at specific activity 110 MBq mg^{-1} . Radiotracer uptake was measured over 10, 20 or 30 min, with up to 15 oocytes in 2 ml transport medium. At the end of the uptake period, oocytes were rinsed twice with ice-cold pH 5.5 medium containing 500 μM unlabeled Fe^{2+} and 1 mM L-ascorbic acid, then solubilized with 5% SDS before ^{55}Fe or ^{65}Zn content was assayed by liquid scintillation counting. Saturation kinetics of $^{55}\text{Fe}^{2+}$ and $^{65}\text{Zn}^{2+}$ uptake were determined using a modified Eq. 1, in which I was replaced with the radiotracer uptake velocity, V .

Intracellular pH recordings

Intracellular pH (pH_i) was measured under voltage clamp using ion-selective microelectrodes as described [3, 10]. Briefly, we used silanized borosilicate micropipettes backfilled with phosphate buffer at pH 7.0, and tips filled with hydrogen ionophore I-cocktail B (Fluka). Electrodes with response > -55 mV/pH unit were selected. The signal from the pH_i electrode was subtracted from the output of the voltage clamp amplifier to yield the responses specifically due to pH. The pH_i and I_m signals were digitized at 0.5 Hz and filtered at 0.05 Hz.

Results

Presteady-state currents associated with wtDMT1 expression in oocytes

Following step changes in membrane potential (V_m) in the *absence* of metal ion, we observed presteady-state currents in oocytes expressing wtDMT1. We did not observe these currents in the *presence* of Fe^{2+} , nor in

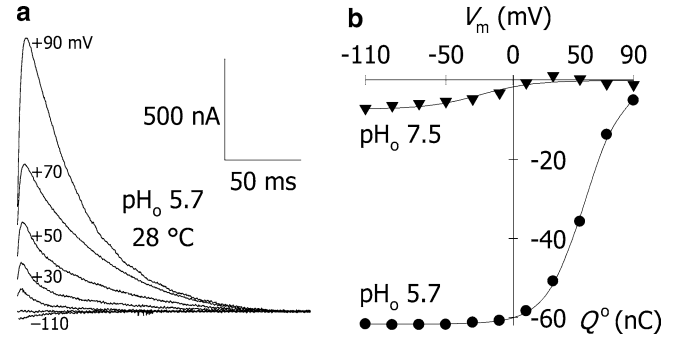


Fig. 1 Presteady-state currents associated with the expression of rat wild type DMT1 (wtDMT1) in *Xenopus* oocytes. **a** Compensated records (from 10 ms after step-changes in V_m from -50 mV to between -110 mV and $+90$ mV were applied) for one oocyte expressing wtDMT1 at pH_o 5.7 and 28°C . For clarity, we show only records at -110 , -50 , $+10$, $+30$, $+50$, $+70$ and $+90$ mV, omitting records at -90 , -70 , -30 , and -10 mV. **b** Presteady-state currents were integrated with time to obtain charge, Q . The Q/V_m relationship at pH_o 5.7 was fit by a single Boltzmann relationship (Eq. 5) with Q_{max} 61.7 ± 1.2 nC, $V_{0.5} + 53.5 \pm 0.9$ mV, and $z - 1.8 \pm 0.1$ ($r^2 = 0.975$). Data obtained at pH_o 7.5 fit a Boltzmann function with Q_{max} 7.3 ± 0.8 nC, $V_{0.5} - 24.5 \pm 8.5$ mV, and $z - 1.3 \pm 0.5$ ($r^2 = 0.759$). For display, data for Q were adjusted to Q° by offsetting to zero the depolarizing limits of Q (Q_{dep}) for each Boltzmann fit (Q_{dep} for pH_o 5.7 was $+61.9 \pm 1.2$ nC, and for pH_o 7.5, $+5.3 \pm 0.6$ nC).

control oocytes. Presteady-state currents were isolated from capacitive transients and steady-state currents (as described in Methods), and are illustrated for a single oocyte superfused at pH_o 5.7, at 28°C (Fig. 1a). Presteady-state currents at pH_o 5.7 decayed with time constants (τ) of 9–31 ms, when fit with a single exponential decay. The relationship of τ to V_m fit a bell-shaped curve with a peak (τ_{max}) of 32.3 ± 0.4 ms at $V_{\tau_{\text{max}}}$ of $+61.1 \pm 0.7$ mV (*not shown*). Presteady-state currents were integrated with time to obtain charge (Q). The relationship of Q to V_m at pH_o 5.7 could be described by a single Boltzmann function (Fig. 1b) with maximal charge movement (Q_{max}) of 62 nC, apparent valence (z) of ≈ -2 , and midpoint of charge transfer ($V_{0.5}$) of $+54$ mV, close to the value obtained for $V_{\tau_{\text{max}}}$. Charge movements were conserved for the onset and offset of step changes in V_m (*not shown*). We observed significantly less charge movement at pH_o 7.5 (Q_{max} was 12 nC) and $V_{0.5}$ was shifted to -25 mV (Fig. 1b).

With the aid of computer simulation, presteady-state currents observed for other H^+ -coupled transporters have been attributed to two steps within the transport cycle, namely (i) reorientation of the empty, charged transporter within the membrane plane and (ii) binding/dissociation of H^+ within the membrane electric field (“ion-well”) [28, 34]. Similar observations have been made in modeling several Na^+ -coupled transporters also [21, 30, 35, 55]. The dependence of both Q_{max} and $V_{0.5}$ upon pH_o suggests that both transporter reorientation and ion-well binding of H^+ contribute to the overall presteady-state charge observed for DMT1. If

H^+ binding were the only transition contributing charge, we would expect that pH_o alter $V_{0.5}$ without effect on Q_{max} (see Ref. [28] for justification). That H^+ may bind to DMT1 in the absence of metal-ion substrate is consistent with observations of a H^+ “leak” (uniport) in the absence of metal ion (see below and Figs. 4, 6) [19, 59].

Iron transport mediated by DMT1: complexation in certain buffers

The uptake of $2 \mu M$ $^{55}Fe^{2+}$ in medium buffered at pH 5.5 using MES and piperazine-1,4-bis(2-propane-sulfonic acid) (PIPPS) was stimulated over 1500-fold in *Xenopus* oocytes expressing wtDMT1 compared with control oocytes (Fig. 2a). Since Tris is known to complex certain metal ions (most notably Cu) [1, 11], we

assessed its impact in our experimental system by comparing $^{55}Fe^{2+}$ uptake in MES/PIPPS-buffered and MES/HEPES/Tris-buffered media. Uptake of $2 \mu M$ $^{55}Fe^{2+}$ in oocytes expressing wtDMT1 was 20% lower in Tris-containing medium at pH 5.5 (Fig. 2a), presumably as a result of complexation of Fe^{2+} . The HEPES (one of several Good’s buffers containing hydroxyalkyl or secondary amine groups) also may complex metal ions [1, 60].

pH-dependence of the Fe^{2+} -evoked currents for DMT1

Since we expected Tris-Fe complexation to be more pronounced at higher pH (as a result of the higher concentration of Tris base; Fig. 2b), we compared the pH-dependence of the Fe^{2+} -evoked currents in media with and without Tris buffer. The currents evoked by $10 \mu M$ Fe^{2+} at -70 mV in the Tris-containing medium appeared to be strictly dependent upon $[H^+]_o$ (Fig. 2b). The data satisfied a conventional 3-parameter Hill function (Eq. 1) with $K_{0.5}^H$ $2.0 \pm 0.8 \mu M$ and Hill coefficient for H^+ , $n_H^H \approx 1$. In contrast, the currents evoked by $10 \mu M$ Fe^{2+} in the Tris-free medium displayed an incomplete dependence upon $[H^+]_o$ (Fig. 2c). Although, the Fe^{2+} -evoked current was stimulated at lower pH_o , significant current remained at neutral pH_o and higher. For example, the Fe^{2+} -evoked current at pH_o 7 (-20 nA) was 21% that at pH_o 5.2 (-95 nA). This raised the possibility that DMT1 can also mediate Fe^{2+} transport that is independent of, or uncoupled from, H^+ , and our subsequent data support this preliminary conclusion.

Why might not the H^+ -independent component of the Fe^{2+} -evoked currents have been apparent when using Tris-containing medium? Presumably this resulted from significant complexation of Fe^{2+} with the higher Tris concentrations necessary to obtain higher pH_o (Fig. 2b). Therefore, we suggest that Tris should be avoided if possible in DMT1 metal-ion transport experiments, and certainly when examining pH-dependence. Yu et al. [60] identified a series of noncomplexing tertiary amine compounds, including the Good’s buffer MES as well as PIPPS (which is now commercially available) that do not complex metal ions. In our subsequent experiments, Fe^{2+} was always presented in Tris-free, MES/PIPPS-buffered media.

The H^+ -dependence data obtained using Tris-free, MES/PIPPS-buffered media could not satisfy a 3-parameter Hill function (Eq. 1) except by constraining the Hill coefficient for H^+ (n_H^H) at 1, yielding $K_{0.5}^H$ of $0.9 \mu M$ and I_{max}^H of -113 nA ($r^2=0.90$) (Fig. 2c, red line). (In initial fits to Eq. 2 or 3, n_H^H was ≈ 1 . Subsequent fits were standardized by constraining n_H^H at 1.) To account for the Fe^{2+} -evoked currents persisting at neutral pH_o or above, we first added a static term, the H^+ -uncoupled current (i^U), to form a 4-parameter Hill function (Eq. 2) that better satisfied the H^+ -dependence

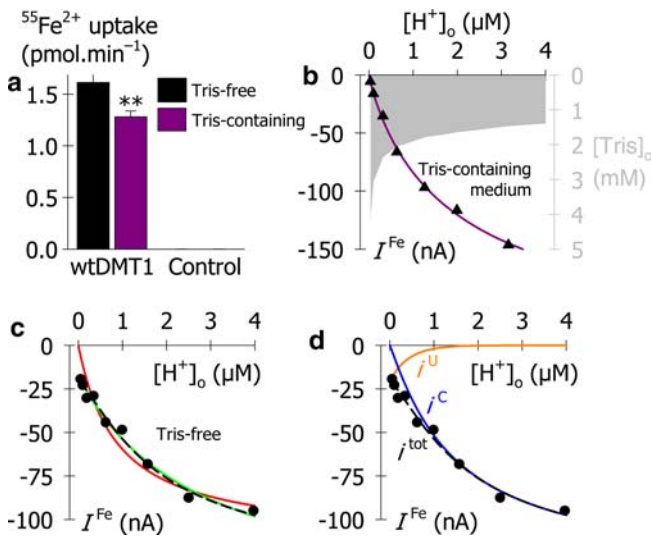


Fig. 2 Effect of buffer composition on iron uptake and H^+ saturation kinetics in oocytes expressing wtDMT1. **a** Uptake of $2 \mu M$ ^{55}Fe was measured over 30 min at pH 5.5 and $21^\circ C$ in control oocytes and oocytes expressing wtDMT1, media buffered using MES and piperazine-1,4-bis(2-propanesulfonic acid) (PIPPS) (black bars) or MES, HEPES, and Tris (purple bars). Data are mean \pm SEM for 7–15 oocytes in each group. $^{**}P < 0.01$, significantly different from uptake in MES/PIPPS buffer. **b, c** H^+ saturation kinetics for wtDMT1 determined from currents evoked by $10 \mu M$ Fe^{2+} at -70 mV, measured in separate wtDMT1-expressing oocytes in the MES/HEPES/Tris buffer system (**b**) or in MES/PIPPS (**c**). Data in **b** were fit with a 3-parameter Hill function (Eq. 1) with $K_{0.5}^H$ $2.0 \pm 0.8 \mu M$, I_{max}^H -243 ± 40 nA, and n_H^H 0.9 ± 0.1 ($r^2=0.998$). The concentration of Tris as a function of pH_o concentration is indicated by the gray shading (right y-axis). Data in **c** were fit with a 3-parameter Hill function (Eq. 1, red line), a 4-parameter Hill function (Eq. 2, green line), and with a function (Eq. 4) combining an exponential decay and a 3-parameter Hill (black dashed line, see **d**). **d** The fit generated by the combined function (Eq. 4, black dashed line, i^{tot}) is separated to display the exponential decay (orange line) describing the currents (i^U) arising from H^+ -uncoupled, facilitative Fe^{2+} transport, and the compensated Hill function (blue line) representing only H^+/Fe^{2+} cotransport currents (i^C). See text for details of derived parameters and fits

data ($r^2=0.98$) and predicted that H^+ -coupled Fe^{2+} transport proceed with $K_{0.5}^H$ of $2.7 \mu M$ and maximal current the sum of I_{max}^H (-136 nA) and the H^+ -uncoupled component i^U (-17 nA) (Fig. 2c, green line). However, we expected that increasing $[H^+]_o$ would accelerate H^+/Fe^{2+} cotransport at the expense of H^+ -uncoupled Fe^{2+} transport. We attempted to describe

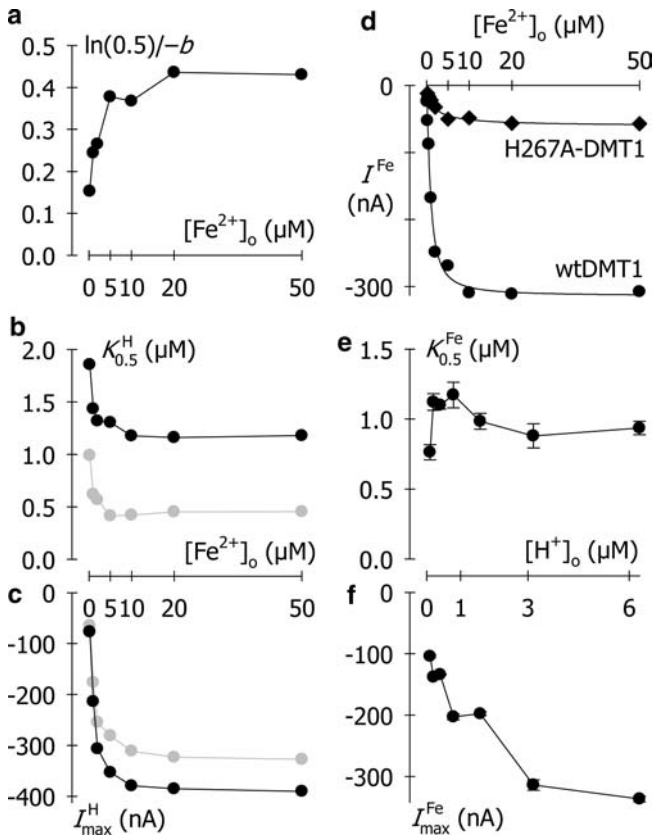


Fig. 3 Fe^{2+} and H^+ saturation kinetics of wtDMT1 as functions of cosubstrate concentrations. Kinetic data for wtDMT1 were derived from the currents evoked by 0.1 – $50 \mu M$ Fe^{2+} at pH_o 5.2 – 7.0 in a single oocyte clamped at V_h -70 mV. The H^+ kinetic parameters as a function of $[Fe^{2+}]_o$ were determined by fitting data with Eq. 3 and as shown in Fig. 2c, d (however data in Fig. 2c are from an independent experiment). **a** The half-maximal H^+ concentration for inhibition of the H^+ -uncoupled, facilitative Fe^{2+} current is given by $\ln(0.5)/-b$, (Eq. 3) and shown as a function of $[Fe^{2+}]_o$. **b, c** Compensated H^+ saturation kinetics ($K_{0.5}$, I_{max}) describing the cotransport currents as a function of $[Fe^{2+}]_o$ (black). For comparison, the parameters derived using a conventional 3-parameter Hill function (Eq. 1) are also indicated (gray). Meanwhile, the pre-exponential value (a) in Eq. 3 can be taken to represent the H^+ -uncoupled, facilitative Fe^{2+} current (i^U) in the theoretical absence of H^+ . These data were plotted as a function of $[Fe^{2+}]_o$ (not shown) and fit to Eq. 1, yielding the following parameters for i^U at $[H^+]_o = 0$: i_{max}^U of -99 ± 2 nA, $K_{0.5}^U$ for Fe^{2+} of $0.61 \pm 0.06 \mu M$, n_H^U for Fe^{2+} of 1.0 ± 0.1 ($r^2 = 0.993$). **d** Fe^{2+} saturation kinetics for wtDMT1 (filled circles) and H267A-DMT1 (filled diamonds) at pH_o 5.5 , -70 mV. Half-maximal Fe^{2+} concentration ($K_{0.5}^{Fe}$) for wtDMT1 was $0.9 \pm 0.1 \mu M$; maximal current (I_{max}^{Fe}) was -314 ± 9 nA; Hill coefficient for Fe^{2+} (n_{Fe}^{Fe}) was 1.3 ± 0.1 ($r^2 = 0.991$). Kinetic parameters for H267A-DMT1 were $K_{0.5}^{Fe}$ $1.5 \pm 0.4 \mu M$, I_{max}^{Fe} -61 ± 4 nA, and n_H^{Fe} 0.9 ± 0.2 ($r^2 = 0.975$). **e, f** Fe^{2+} saturation kinetics ($K_{0.5}$, I_{max}) as a function of pH_o . Error bars represent the standard error of regression

this effect by modifying i^U with an exponential decay which, when combined with the Hill function (Eq. 3), resulted in a further increase in the regression coefficient ($r^2=0.99$) (Fig. 2c, dashed black line). Similar findings were obtained in four independent preparations (not shown). Whereas the fit resembled that for Eq. 2, the alternative prediction of the behavior of the H^+ -uncoupled component resulted in different values for the H^+ saturation kinetics of the coupled Fe^{2+} currents (Fig. 2d, blue line), $K_{0.5}^H$ of $1.6 \mu M$ and I_{max}^H of -139 nA. Meanwhile, the H^+ -uncoupled Fe^{2+} current (Fig. 2d, orange line) was described by its pre-exponential factor (a) of -19 nA, and the midpoint ($\ln(0.5)/-b$) of its inhibition by H^+ at $[H^+]_o = 0.28 \mu M$ (i.e. pH_o 6.5). On the basis of the improved regressions, and the theoretical interpretation of these and other data presented in support of DMT1-mediated facilitative Fe^{2+} transport that is uncoupled from H^+ (see model in Fig. 8), we suggest that Eq. 3 may provide the most reliable estimates of H^+ saturation kinetic parameters.

Binding order and transport mechanism of DMT1

In order to explore the substrate binding order and transport mechanism of DMT1, we examined both the H^+ and Fe^{2+} saturation kinetics as a function of cosubstrate concentrations at -70 mV (Fig. 3). The H^+ -dependence data were fit with Eq. 3 (as in Fig. 2c, d) at each Fe^{2+} concentration from 0.2 to $50 \mu M$. The H^+ concentration at which the uncoupled Fe^{2+} current was inhibited 50% (i.e. $\ln(0.5)/-b$) increased with increasing Fe^{2+} concentration (Fig. 3a), evidence that H^+ and Fe^{2+} may compete for the unloaded transporter. The $K_{0.5}^H$ describing H^+/Fe^{2+} cotransport was lowest ($1.2 \mu M$) at high Fe^{2+} concentration and rose to $1.9 \mu M$ at low Fe^{2+} concentration, consistent with a simultaneous transport mechanism [25, 28, 35, 36, 49]. That is, H^+ and Fe^{2+} are translocated within the same transport cycle when both substrates are present. In contrast, $K_{0.5}^H$ would be expected to increase at higher Fe^{2+} concentrations if H^+ and Fe^{2+} were transported consecutively [25, 49]. The I_{max}^H was maximal when Fe^{2+} concentrations were saturating (Fig. 3c), but was significantly reduced at lower Fe^{2+} concentrations. Thus, Fe^{2+} concentration limited the maximal rate of cotransport, consistent with ordered binding of H^+ then Fe^{2+} [25, 35, 36, 49]. Fitting our data using the combined function (Eq. 3) resulted in quantitative differences $K_{0.5}^H$ and I_{max}^H —but no qualitative difference in their behavior as a function of $[Fe^{2+}]_o$ —relative to the values generated from the conventional 3-parameter Hill function (Eq. 1) (Fig. 2b, c). However, since Eq. 3 also accounts for the facilitative component of the Fe^{2+} -evoked currents, we anticipate that fitting to Eq. 3 provides more appropriate $K_{0.5}^H$ and I_{max}^H values. When n_H^H was not constrained in Eq. 3, n_H^H was 0.9 – 1.3 and did not vary with Fe^{2+} concentration, indicating that the binding of only one H^+ is required to activate the

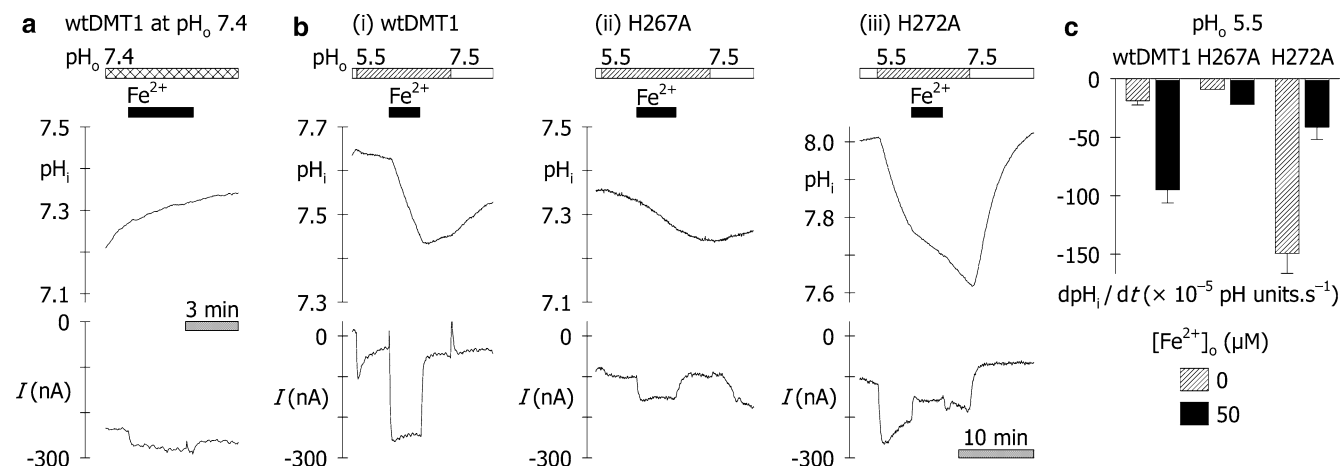


Fig. 4 Changes in intracellular pH (pH_i) associated with DMT1 activity in oocytes expressing wild type and mutant DMT1. **a**, **b** pH_i changes (upper panels) and currents (lower panels) were recorded simultaneously in individual oocytes voltage-clamped at $V_h = -90$ mV. **a** An oocyte expressing wtDMT1 was superfused at pH_o 7.4 (cross-hatched bar) and 50 μM Fe^{2+} added for the period shown by the filled box. The Fe^{2+} evoked a small inward current that was not associated with intracellular acidification. **b** Oocytes were superfused with pH 7.5 medium (blank boxes), then

pH 5.5 medium (hatched boxes), and 50 μM Fe^{2+} at pH_o 5.5 (filled boxes). Typical records are shown for oocytes expressing (i) wtDMT1, (ii) H267A-DMT1, and (iii) H272A-DMT1. The 10 min scale bar refers to all panels in **b**. **c** Summary of acidification rates for all oocytes tested at pH_o 5.5. The rate of intracellular acidification (dpH_i/dt) was calculated after switching from pH_o 7.5 to 5.5 (hatched bars) and upon adding 50 μM Fe^{2+} at pH_o 5.5 (solid bars). Data are mean \pm SEM for wtDMT1 ($n = 7$) and H272A ($n = 3$). Data for H267A are from a single oocyte

cotransport cycle, or that there is no cooperativity between multiple binding sites. However, the Hill coefficient is not a direct index of coupling stoichiometry in transporters, and the H^+/Fe^{2+} stoichiometry of DMT1 is not fixed. Significant slippage is evident, with H^+ fluxes generally exceeding the fluxes of Fe^{2+} [7, 59].

The Fe^{2+} -evoked currents also were saturable. In a typical example, at $V_h = -70$ mV and pH_o 5.5, the half-maximal Fe^{2+} concentration ($K_{0.5}^{Fe}$) was 0.9 ± 0.1 μM (Fig. 3d). The Hill coefficient for Fe^{2+} (n_H^{Fe}) was close to 1 and was independent of pH_o (not shown), suggesting that only one Fe^{2+} is involved in each transport cycle. The relationship of $K_{0.5}^{Fe}$ to H^+ concentration was biphasic (Fig. 3e): at low H^+ concentrations, $K_{0.5}^{Fe}$ rose significantly from 0.8 μM at

neutral pH_o to 1.2 μM at pH_o 6.1, further evidence that Fe^{2+} and H^+ compete at higher pH_o . However, $K_{0.5}^{Fe}$ fell again (to 0.9 μM) at higher H^+ concentrations, consistent with simultaneous translocation of substrates at low pH_o .

We would expect I_{max}^{Fe} to be independent of H^+ concentration if H^+ binds first in a strict cotransport model, so that saturating Fe^{2+} should always drive the transporter at maximal velocity regardless of H^+ concentration [25, 35, 36, 49]. However, I_{max}^{Fe} was markedly dependent upon H^+ concentration (Fig. 3f), consistent with a H^+ -uncoupled, facilitative Fe^{2+} transport pathway short-circuiting cotransport at high pH_o . These data indicate that, at low pH_o , H^+ binding precedes Fe^{2+} binding and its simultaneous transport

Table 2 Summary of analysis of rat wild type DMT1, and the His-267 and His-272 mutants

Protein	Q_{max} (nC) ^a	I_{max}^{Fe} (nA) ^b	Turnover rate (s^{-1}) ^c	Transporter density (N_T) ^d	$K_{0.5}^{Fe}$ (μM) ^e	Substrate preference	$K_{0.5}^H$ of cotransport (μM) ^f	$K_{0.5}^H$ of leak (μM) ^g
WtDMT1	48 ± 3	-1002	21	3.2×10^{11} /oocyte	0.9 ± 0.1	$Fe^{2+} >> Zn^{2+}$	1.4 ± 0.2	—
H267A	23 ± 1	-515	23	1.3×10^{11} /oocyte	1.5 ± 0.4	—	—	—
H267D	< 2	-6	—	—	—	—	—	—
H267N	6 ± 1	-74	12	0.4×10^{11} /oocyte	< 5	—	—	—
H272A	None detected	+83	—	—	0.36 ± 0.06 (K_i^{Fe})	$Fe^{2+} = Zn^{2+}$	NA	2.2 ± 0.3
H272R	None detected	+186	—	—	—	—	NA	—

^a Total presteady-state charge (Q_{max}) determined using Eq. 4, at pH_o 5.5 and 23°C (data are from a different preparation than that used in Fig. 1). In the case of H267D, presteady-state currents were visible but smaller than could be isolated satisfactorily from capacitive currents. In the case of H272A and H272R, no presteady-state currents were visible

^b Current evoked by 50 μM Fe^{2+} at pH_o 5.5, 23°C, and -150 mV (Fig. 5a) in the same oocytes in which we determined Q_{max}

^c Turnover rate determined as I_{max}/Q_{max} (under the conditions defined here separately for Q_{max} and $I_{max}^{a,b}$)

^d Transporter density determined according to Eq. 6

^e $K_{0.5}^{Fe}$ determined at pH_o 5.5 and -70 mV; in the case of H272A, the value given is K_i^{Fe} , the Fe^{2+} concentration at which the H^+ leak was inhibited by 50%

^f $K_{0.5}^H$ determined at 10 μM Fe^{2+} and -50 mV, mean of three oocytes^g $K_{0.5}^H$ of the H^+ leak pathway determined at -50 mV/NA not applicable

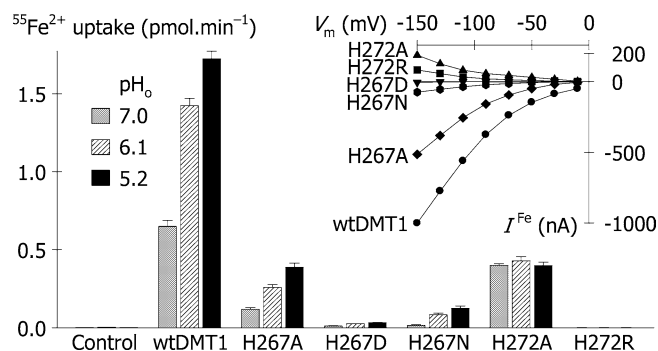


Fig. 5 Fe^{2+} transport mediated by wtDMT1 and histidyl mutants: effects of alternative substitutions. The pH-dependence of $2 \mu\text{M}$ $^{55}\text{Fe}^{2+}$ uptake, determined over 30 min. Data are mean \pm SEM for 7–15 oocytes in each group. *Inset* Current/voltage relationships for $50 \mu\text{M}$ Fe^{2+} superfused at pH_o 5.5. Inward currents were observed for wtDMT1 (circles), H267A (diamonds), H267N (hexagons), and H267D (inverted triangles). Outward currents, presumably representing inhibition of the H^+ leak by Fe^{2+} , were observed for H272A (triangles) and H272R (squares). Currents derive from a separate oocyte preparation from that in which we measured $^{55}\text{Fe}^{2+}$ uptake (main figure)

across the membrane. However, around neutral pH_o, wtDMT1 binds and transports Fe^{2+} independent of H^+ . Additionally, H^+ binding and translocation may proceed at low pH_o in the complete absence of metal ion (i.e. H^+ leak), as evidenced by the modest intracellular acidification and small inward current detected upon switching from pH_o 7.5 to 5.5 prior to adding metal ion (see Fig. 4b(i)).

Fe^{2+} transport at pH_o 7.4 is not accompanied by H^+ influx

We showed previously that the Fe^{2+} -evoked current in DMT1-expressing oocytes at pH_o 5.5 was associated with a rapid intracellular acidification, consistent with H^+ -coupled Fe^{2+} transport [19]. Here, we superfused DMT1-expressing oocytes in the absence of an inwardly directed H^+ chemical gradient (pH_o was 7.4), we found that $50 \mu\text{M}$ Fe^{2+} evoked a modest but significant inward current that was not accompanied by a H^+ influx.

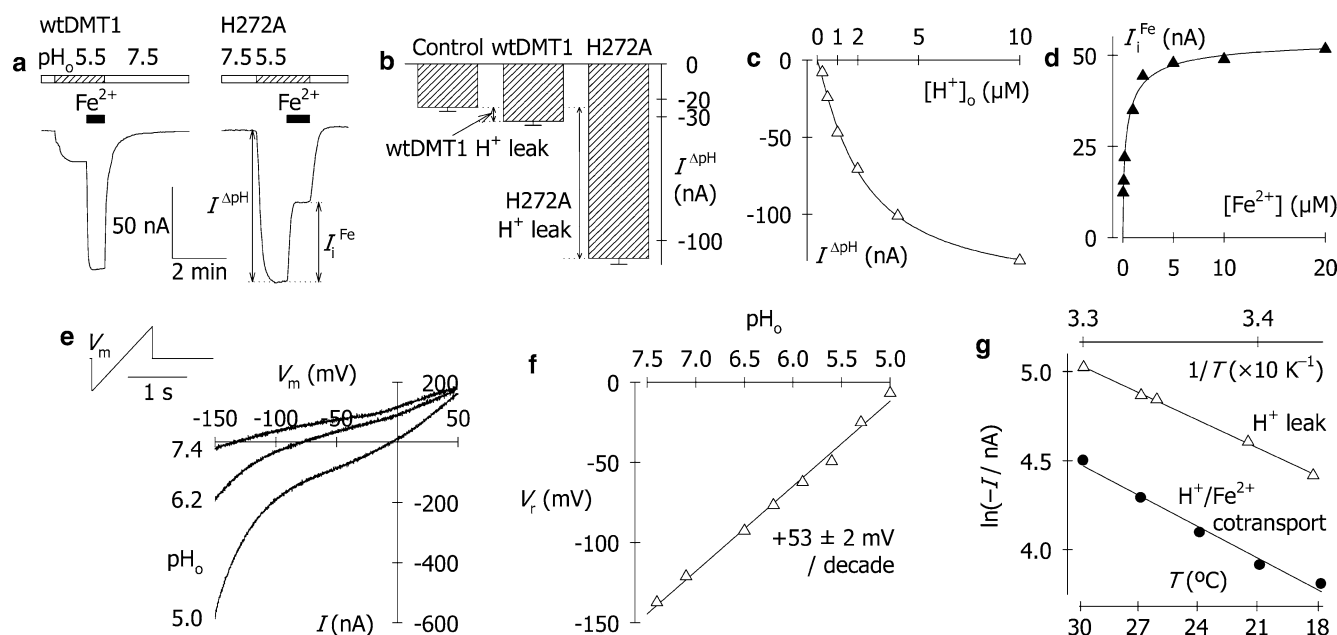


Fig. 6 Properties of a leak current mediated by H272A-DMT1. **a** Typical current records at -50 mV for wtDMT1 and H272A-DMT1 first superfused with pH 7.5 medium (blank boxes), then pH 5.5 medium (hatched boxes), and the effect of adding $50 \mu\text{M}$ Fe^{2+} (black boxes). Indicated are the magnitudes of the inward current ($I^{\Delta\text{pH}}$) resulting from switching from pH_o 7.5–5.5, and the Fe^{2+} -induced inhibition current (I^{Fe}) in H272A. **b** Leak currents associated with expression of wtDMT1 and H272A-DMT1 in oocytes, quantified as $I^{\Delta\text{pH}}$ (see **a**) less that observed for control oocytes. Data are mean \pm SEM for 7–12 oocytes. **c** H^+ saturation of the leak current mediated by H272A-DMT1. Data were fit with Eq. 2, from which we obtained $K_{0.5}^{\text{H}}$ $2.2 \pm 0.3 \mu\text{M}$, $I_{\text{max}}^{\text{H}}$ $-152 \pm 9 \text{ nA}$, and n_{H}^{H} 1.2 ± 0.1 ($r^2 = 0.998$). **d** Fe^{2+} -induced inhibition current (I^{Fe}) in H272A (see **a**). The Fe^{2+} -induced inhibition current mediated by H272A-DMT1 was inhibited by Fe^{2+} with K_i^{Fe} of $0.2 \pm 0.1 \mu\text{M}$ (other parameters from the fit to Eq. 2 were $I_{\text{max}}^{\text{Fe}}$ $+55 \pm 2 \text{ nA}$, n_{H}^{Fe} 0.7 ± 0.1 , $r^2 = 0.994$). **e** A 1 s voltage ramp protocol (inset) was applied in an oocyte expressing H272A-DMT1 to determine reversal potential (V_r) as a function of pH_o, plotted in

f. For clarity, only the records at pH_o 7.4, 6.2, and 5.0 are displayed. **f** V_r of the leak currents for H272A-DMT1 as a function of pH_o. The V_r shifted to depolarized V_m with increasing $[\text{H}^+]_o$, with a slope of $+53 \pm 2 \text{ mV}$ per decade ($r^2 = 0.994$). **g** The temperature dependence of the H^+ leak was determined as $I^{\Delta\text{pH}}$ mediated by H272A-DMT1 (filled triangles) at pH_o 5.7 and -50 mV , after subtracting the endogenous H^+ currents determined in a control oocyte from the same batch (not shown, these were 12–15% the magnitude of the H^+ currents in the oocyte expressing H272A-DMT1). The temperature dependence of H^+ /Fe²⁺ cotransport was determined as the current evoked by $50 \mu\text{M}$ Fe^{2+} in an oocyte expressing wtDMT1 (filled circles) at pH_o 5.7 and -50 mV . Arrhenius transformation (Eq. 4) yielded activation energy (E_a) of $10.3 \pm 0.2 \text{ kcal mol}^{-1}$ for wild type H^+ /Fe²⁺ cotransport ($\ln A = 21.6 \pm 1.3$; $r^2 = 0.985$). E_a for the H^+ leak mediated by H272A-DMT1 was $9.1 \pm 0.2 \text{ kcal mol}^{-1}$ ($\ln A = 20.1 \pm 0.3$; $r^2 = 0.999$). (Endogenous H^+ currents in a control oocyte had $E_a = 5.9 \pm 0.4 \text{ kcal mol}^{-1}$, $\ln A = 13.0 \pm 0.6$; $r^2 = 0.989$)

We confirmed this observation for three individual oocytes at pH_o 7.4, and a representative record is shown in Fig. 4a. In contrast, when we imposed an inwardly directed H^+ chemical gradient (pH_o 5.5), the larger Fe^{2+} -evoked current was associated with significant intracellular acidification (Fig. 4b(i)). These observations support our conclusion that Fe^{2+} transport at neutral pH_o or above is predominantly uncoupled from H^+ .

Impact of mutations in DMT1 at His-267 and His-272

We then evaluated the impact of mutations in DMT1 at His-267 and His-272 in putative TM6 [33]. The remaining seven histidyl residues in DMT1 are thought to reside in the intracellular *N*-terminal region, or in intracellular or extracellular loops. Histidyl residues are common targets for transporter mutagenesis, and we considered the possibilities that His-267 and His-272 may interact with H^+ or—as a pair—form a metal-

binding site. The H267A-DMT1, when expressed in oocytes, displayed properties similar to those of wtDMT1 (summarized in Table 2), but at a lower level. However, the H272A mutation resulted in striking changes in the activity of the protein.

Analysis of H267A-DMT1

The Fe^{2+} evoked currents of up to -500 nA at pH_o 5.5 in oocytes expressing H267A-DMT1, and the current/voltage relationship resembled that of wtDMT1 (Fig. 5, inset). The smaller Fe^{2+} -evoked currents observed for H267A-DMT1 compared with wtDMT1 correlated with the reduced transporter density (estimated from pre-steady-state currents) for H267A-DMT1 in the oocyte membrane (Table 2). The turnover rate for H267A-DMT1 was 23 s^{-1} , and that for wtDMT1 was 21 s^{-1} , indicating that the smaller currents observed for H267A-DMT1 did not result from reduced transporter effi-

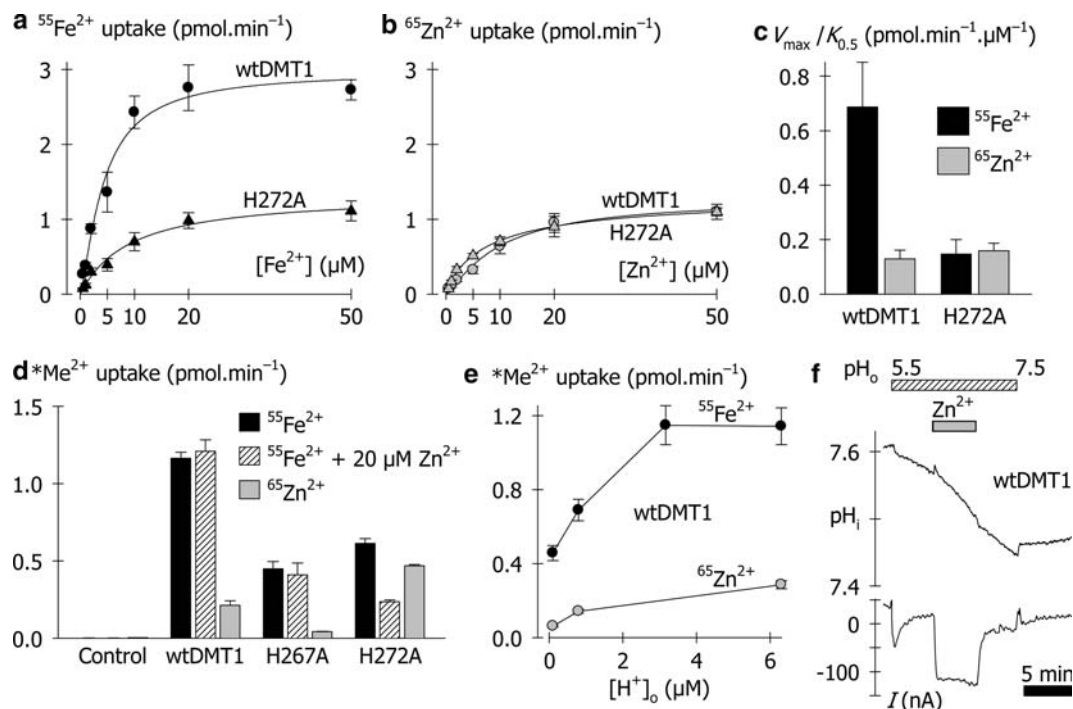


Fig. 7 Comparison of Fe^{2+} and Zn^{2+} transport mediated by wtDMT1 and DMT1 mutants. **a** Concentration dependence of $^{55}\text{Fe}^{2+}$ uptake, measured over 10 min at pH_o 5.5. Data for wtDMT1 (black circles) were fit with Eq. 1 to determine Fe^{2+} transport kinetic parameters: $V_{\text{max}}^{\text{Fe}}$ $3.0 \pm 0.3 \text{ pmol min}^{-1}$, $K_{0.5}^{\text{Fe}}$ $4.3 \pm 0.9 \mu\text{M}$, and Hill coefficient for Fe^{2+} (n_{H}^{Fe}) 1.3 ± 0.3 ($r^2 = 0.977$). For H272A-DMT1 (black triangles): $V_{\text{max}}^{\text{Fe}}$ $1.3 \pm 0.2 \text{ pmol min}^{-1}$, $K_{0.5}^{\text{Fe}}$ $9.1 \pm 3.1 \mu\text{M}$, and n_{H}^{Fe} 1.0 ± 0.2 ($r^2 = 0.985$). **b** Concentration dependence of $^{65}\text{Zn}^{2+}$ uptake over 10 min under the same experimental conditions, set to the same scaling, and in oocytes from the same preparation as in (a). Data were fit with Eq. 1, for wtDMT1 (gray circles): $V_{\text{max}}^{\text{Zn}}$ $1.3 \pm 0.1 \text{ pmol min}^{-1}$, $K_{0.5}^{\text{Zn}}$ $9.9 \pm 2.3 \mu\text{M}$, and n_{H}^{Zn} 1.2 ± 0.2 ($r^2 = 0.989$), and for H272A-DMT1 (gray triangles): $V_{\text{max}}^{\text{Zn}}$ $1.3 \pm 0.1 \text{ pmol min}^{-1}$, $K_{0.5}^{\text{Zn}}$ $8.3 \pm 1.4 \mu\text{M}$, n_{H}^{Zn} 0.9 ± 0.1 ($r^2 = 0.998$). Each data point in A and B represents mean

\pm SEM for 6–11 oocytes. **c** $I_{\text{max}}/K_{0.5}$ as an index of transport efficiency, using kinetic parameters from $^{55}\text{Fe}^{2+}$ and $^{65}\text{Zn}^{2+}$ uptake data in A and B, for wtDMT1 and H272A-DMT1. Error bars were propagated from the standard errors of regression. **d** Radiotracer metal-ion ($^*\text{Me}^{2+}$) uptake mediated by wtDMT1, and the H267A and H272A mutants. Uptake of $2 \mu\text{M}$ $^{55}\text{Fe}^{2+}$ in the absence (black bars) or presence (hatched bars) of $20 \mu\text{M}$ Zn^{2+} , and uptake of $2 \mu\text{M}$ $^{65}\text{Zn}^{2+}$ (gray bars), were measured over 10 min at pH_o 5.5. Data are mean \pm SEM for 7–14 oocytes. **e** Wildtype DMT1-mediated uptake of $2 \mu\text{M}$ $^{55}\text{Fe}^{2+}$ (black circles) and $2 \mu\text{M}$ $^{65}\text{Zn}^{2+}$ (gray circles) over 10 min as a function of extracellular pH (pH_o). Data are mean \pm SEM for 6–13 oocytes. **f** Effect of Zn^{2+} on intracellular pH (pH_i) in an oocyte expressing wtDMT1, superfused with pH 7.5 medium (blank boxes), then pH 5.5 (hatched boxes). $50 \mu\text{M}$ Zn^{2+} was superfused (at pH_o 5.5) for the period shown by the gray box

ciency. The Fe^{2+} -evoked currents in oocytes expressing H267A-DMT1 were saturable, with $K_{0.5}^{\text{Fe}}$ of $1.5 \pm 0.4 \mu\text{M}$ (Fig. 3d), close to that observed for wtDMT1 ($\approx 1 \mu\text{M}$). The Fe^{2+} transport mediated by H267A-DMT1 was associated with a modest H^+ influx (Fig. 4b(ii)), and $^{55}\text{Fe}^{2+}$ uptake mediated by H267A-DMT1 displayed a pH-dependence similar to that of wtDMT1 (Fig. 5). Therefore, although the H267A mutant is expressed at lower levels in the oocyte plasma membrane, the properties of H267A-DMT1 closely resemble those of wtDMT1. Nevertheless, additional effects may be expected when both His-267 and His-272 are mutated together [29].

Analysis of H272A-DMT1

As previously observed [19, 59], wtDMT1 mediated a modest, 'leak' current upon switching from pH_o 7.5 to 5.5 in the absence of metal ion (Figs. 4b(i), c, 6a). The resulting H^+ -induced inward current (I^{APH}) exceeded by about 10 nA that observed in control oocytes (Fig. 6b) and was associated with a modest intracellular acidification (Fig. 4b(i)). Addition of Fe^{2+} resulted in a much more rapid acidification and a much larger inward current (Figs. 4b(i), c, 6a). In contrast, H272A-DMT1 mediated a significant leak current (approximately tenfold that observed for wtDMT1) and this leak current was inhibited by Fe^{2+} (Figs. 4b(iii), c, 6a, b). The leak in H272A-DMT1 was associated with a rapid intracellular acidification (Fig. 4b(iii)) that was significantly slowed by $72 \pm 20\%$ upon the addition of Fe^{2+} (Fig. 4c). The slowing of acidification rate with Fe^{2+} was not the result of intracellular buffering in the oocyte, since removal of the Fe^{2+} again accelerated the intracellular acidification at pH_o 5.5 (Fig. 4b(iii)). As for wtDMT1, the inward currents and changes in intracellular pH observed for H272A-DMT1 were reversed upon returning to pH_o 7.5 (Fig. 4b(i), (iii)).

The H272A-DMT1-mediated leak current was inhibited by Fe^{2+} with apparent $K_i^{\text{Fe}} \approx 0.4 \mu\text{M}$. This value may be a better reflection of the affinity at which DMT1 binds Fe^{2+} than is the Fe^{2+} concentration at which wtDMT1-mediated transport is half-maximal (i.e. $K_{0.5}^{\text{Fe}}$), since $K_{0.5}^{\text{Fe}}$ —but not K_i^{Fe} —additionally describes the complete transport cycle. Supersaturating Fe^{2+} ($50 \mu\text{M}$) did not fully reverse the inward leak current associated with H272A-DMT1 (Figs. 4, 6a, c, d), indicating either that inhibition of the leak by Fe^{2+} is incomplete, or that Fe^{2+} is itself transported by H272A-DMT1, resulting in a residual inward current, a conclusion supported by the significant $^{55}\text{Fe}^{2+}$ uptake we observed in oocytes expressing H272A-DMT1 (Fig. 5). Notably, however, the $^{55}\text{Fe}^{2+}$ uptake mediated by H272A-DMT1 was independent of pH_o (7.0, 6.1, or 5.2), whereas wtDMT1-mediated $^{55}\text{Fe}^{2+}$ uptake was markedly stimulated at low pH_o (Figs. 5, 7e). Since H272A-DMT1 mediated a substantially increased leak current as well as pH-independent Fe^{2+} transport, we conclude

that the major impact of the H272A mutation was an uncoupling of Fe^{2+} transport from the H^+ flux. The $K_{0.5}^{\text{Fe}}$ for H272A-DMT1 at pH_o 5.5 was $\approx 9 \mu\text{M}$ (Fig. 7b), similar to the $K_{0.5}^{\text{Fe}}$ of $7.2 \mu\text{M}$ derived for wtDMT1 at pH_o 7.0 (*not shown*). These observations provide evidence that the DMT1 protein possesses the machinery for facilitative Fe^{2+} transport, uncoupled from H^+ .

Properties of the leak current mediated by H272A-DMT1

Given its substantially larger leak current and the uncoupling of Fe^{2+} and H^+ fluxes, H272A-DMT1 can serve as a model system in which to study the DMT1-mediated leak. In oocytes expressing H272A-DMT1, I^{APH} (which largely represents the H272A-DMT1-mediated leak since I^{APH} in control oocytes was around -20 nA) was dependent on the final pH_o . The relationship of I^{APH} to extracellular H^+ concentration fit a Hill function (Eq. 1) with Hill coefficient (n_H) ≈ 1 (Fig. 6c), as for cotransport. The $K_{0.5}^{\text{H}}$ of $\approx 2 \mu\text{M}$ for the leak is similar to the $K_{0.5}^{\text{H}}$ ($1\text{--}2 \mu\text{M}$) for wtDMT1 Fe^{2+} -evoked currents (Figs. 3b, 6c). We applied a voltage-ramp protocol to determine the reversal potential (V_r) as a function of pH_o in oocytes expressing H272A-DMT1 (Fig. 6e, f). The V_r varied from -137 mV at pH_o 7.4 to -6 mV at pH_o 5.0 (Fig. 6f). The slope of V_r as a function of pH_o was $+53 \text{ mV per pH}_o$ unit, close to the slope of $+58 \text{ mV per pH}_o$ unit predicted from the Nernst equation (at 22°C), indicating that the H272A-DMT1-mediated leak current is carried solely by H^+ . This observation is consistent with the intracellular acidification observed upon switching from pH_o 7.5 to 5.5 for H272A-DMT1 (Fig. 5) and, although less markedly, also for wtDMT1 (Figs. 5, 7f). The wtDMT1-mediated Fe^{2+} -evoked currents were temperature-dependent, with Arrhenius activation energy (E_a) of $\approx 10 \text{ kcal mol}^{-1}$ (Fig. 6g). The H272A-DMT1-mediated H^+ leak currents displayed a similar temperature dependence with $E_a \approx 9 \text{ kcal mol}^{-1}$, suggesting that H^+ uniport (leak)—like wild type cotransport—is carrier-mediated and involves substantial conformational changes. In contrast, if the leak were channel-mediated, we would expect the H^+ leak to have activation energy lower than that for cotransport. That the parameters n_H and $K_{0.5}^{\text{H}}$ do not differ for the H^+ leak and cotransport pathways suggests a common H^+ binding site.

Impact of alternative substitutions at His-267 and His-272

We examined the impact of additional substitutions at histidyl residues 267 and 272. Substitution of His-267 with asparagine (N) or aspartic acid (D) resulted in activities that were qualitatively similar to wtDMT1 and H267A-DMT1, but with significantly reduced expres-

sion of functional units at the plasma membrane (Table 2). Based on $^{55}\text{Fe}^{2+}$ uptake and Fe^{2+} -evoked currents (Fig. 5), Fe^{2+} transport in oocytes expressing H267N-DMT1 was dependent on both pH_o and membrane potential. $K_{0.5}^{\text{Fe}}$ was $<5\text{ }\mu\text{M}$ (since 5, 50 and $500\text{ }\mu\text{M}$ Fe^{2+} evoked similar currents -20 , -17 nA , and -19 nA , respectively, at -50 mV and $\text{pH}_o\text{ }5.5$, *not shown*). The H267N-DMT1 also displayed presteady-state currents (*not shown*), with $V_{0.5} = +30 \pm 2\text{ mV}$, $z = -1.0 \pm 0.1$ ($r^2 = 0.921$). The Q_{max} of $6 \pm 1\text{ nC}$ was only 13% of that for wtDMT1 (Table 2). The H267N-DMT1 turnover rate was lower than for wtDMT1 (Table 2) but our confidence in this value for H267N-DMT1 is limited since both the presteady-state currents and Fe^{2+} -evoked currents were so small. The H267D-DMT1 exhibited even lower activity, in keeping with the tiny presteady-state currents observed for that mutant (too small to reliably isolate from capacitive currents). The H267D-DMT1 mediated pH-dependent $^{55}\text{Fe}^{2+}$ uptake that exceeded that observed for control oocytes, in addition to Fe^{2+} -evoked inward currents that were barely discernible (Fig. 5).

We mutated His-272 to an arginine (R) residue (i.e. permanently cationic, rather than titratable within the physiological pH_o range). Like H272A, the H272R mutation abolished presteady-state currents (*not shown*) and mediated a small Fe^{2+} -inhibitable H^+ leak (*not shown*). The inhibition of the H^+ leak underlies the small outward currents observed in the presence of Fe^{2+} at $\text{pH}_o\text{ }5.5$ (Fig. 5 inset). However, whereas H272A-DMT1 also mediated pH-independent Fe^{2+} transport, H272R-DMT1 did not mediate any $^{55}\text{Fe}^{2+}$ transport activity (Fig. 5).

Comparison of zinc and iron transport mediated by DMT1

The wtDMT1 also transported Zn^{2+} but at much lower maximal velocity (V_{max}) and with lower apparent affinity than wtDMT1-mediated Fe^{2+} transport. The V_{max} for $^{65}\text{Zn}^{2+}$ uptake in oocytes expressing wtDMT1 was only 43% the V_{max} for $^{55}\text{Fe}^{2+}$ uptake (Fig. 7a, b). Meanwhile, the zinc concentration at which uptake was half-maximal ($K_{0.5}^{\text{Zn}} = 9.9\text{ }\mu\text{M}$) was more than double the $K_{0.5}^{\text{Fe}}$ ($4.3\text{ }\mu\text{M}$). Taking the ratio $V_{\text{max}}/K_{0.5}$ as an index of the efficiency with which each metal ion is transported by wtDMT1, wtDMT1 displayed a fivefold preference for Fe^{2+} over Zn^{2+} (Fig. 7c). The H272A mutation significantly affected Fe^{2+} transport, both reducing $I_{\text{max}}^{\text{Fe}}$ and increasing $K_{0.5}^{\text{Fe}}$ compared with wtDMT1, without impact on zinc transport (Fig. 7a, b). Thus, the H272A mutation abolished the marked preference for Fe^{2+} over Zn^{2+} (Fig. 7c).

Subsaturating Zn^{2+} failed to inhibit the uptake of $2\text{ }\mu\text{M}$ $^{55}\text{Fe}^{2+}$ in oocytes expressing wtDMT1 (or H267A-DMT1), but significantly inhibited $^{55}\text{Fe}^{2+}$ uptake in oocytes expressing H272A-DMT1 (Fig. 7d). The H272A-DMT1 transported $2\text{ }\mu\text{M}$ $^{65}\text{Zn}^{2+}$ and $^{55}\text{Fe}^{2+}$

equally well, whereas uptake of $2\text{ }\mu\text{M}$ $^{55}\text{Fe}^{2+}$ greatly exceeded that of $^{65}\text{Zn}^{2+}$ in oocytes expressing wtDMT1 or H267A-DMT1 (Fig. 7d). That H272A-DMT1 (in which metal-ion transport is uncoupled from H^+) did not exhibit the marked preference for Fe^{2+} over Zn^{2+} displayed by wtDMT1 led us to consider the possibility that Zn^{2+} may be transported only by the H^+ -uncoupled, facilitative metal-ion pathway in DMT1, and that the H^+ -coupled and H^+ -uncoupled pathways could differ in their metal-ion selectivity. However, examination of the pH-dependence and H^+ -coupling of Zn^{2+} transport mediated by wtDMT1 revealed that uptake of $2\text{ }\mu\text{M}$ $^{65}\text{Zn}^{2+}$ was accelerated at low pH_o , as was $^{55}\text{Fe}^{2+}$ uptake (Fig. 7e).

Consistent with Fe^{2+} -evoked currents (Fig. 2c), significant $^{55}\text{Fe}^{2+}$ uptake persisted at $\text{pH}_o\text{ }7.0$, further supporting our conclusion that DMT1 can also mediate H^+ -uncoupled facilitative Fe^{2+} transport. Meanwhile, H^+ -coupled $^{55}\text{Fe}^{2+}$ transport (at $2\text{ }\mu\text{M}$ Fe^{2+}) proceeded with $K_{0.5}^{\text{H}}$ of $1\text{--}3\text{ }\mu\text{M}$ (estimated from Fig. 7e), close to that determined from Fe^{2+} -evoked currents ($K_{0.5}^{\text{H}} = 1\text{--}2\text{ }\mu\text{M}$; see Fig. 3b). The $K_{0.5}^{\text{H}}$ for $^{65}\text{Zn}^{2+}$ transport was on the order of that for $^{55}\text{Fe}^{2+}$ transport (Fig. 7e). In an oocyte expressing wtDMT1, superfusing $50\text{ }\mu\text{M}$ Zn^{2+} resulted in an inward current and a modest acceleration of intracellular acidification compared with that induced by low pH_o alone (Fig. 7f). Removing the Zn^{2+} slowed the intracellular acidification. The Zn^{2+} -induced acidification in this oocyte was much slower ($-28 \times 10^{-5}\text{ pH units s}^{-1}$) than that induced by Fe^{2+} ($-95 \times 10^{-5} \pm 11 \times 10^{-5}\text{ pH units s}^{-1}$, $n = 7$; see Fig. 4c), but consistent with the lower uptake rates observed for $^{65}\text{Zn}^{2+}$. These data indicate that DMT1-mediated Zn^{2+} transport at low pH_o is H^+ -coupled, like Fe^{2+} transport, and do not support the idea that Zn^{2+} transport is limited to the H^+ -uncoupled, facilitative transport pathway in DMT1.

Discussion

DMT1-mediated Fe^{2+} transport is stimulated by the H^+ electrochemical potential gradient

The DMT1-mediated Fe^{2+} transport is H^+ -coupled, driven by the H^+ electrochemical potential gradient. However, coupling is not strict, and significant slippage may occur. Evidence for H^+ -coupling includes our observations in oocytes expressing wtDMT1 that (i) the $V_{0.5}$ (midpoint) of the presteady-state charge transfer in the absence of metal ion was pH_o -sensitive (Fig. 1), supporting binding/dissociation of H^+ ; (ii) $^{55}\text{Fe}^{2+}$ uptake and Fe^{2+} -evoked currents were stimulated at low pH_o (Figs. 2, 5, 7e); (iii) Fe^{2+} transport at low pH_o was associated with rapid intracellular acidification (Fig. 4b, c). The Fe^{2+} -evoked currents had no pH_o optimum, but followed Michaelis–Menten-type saturation kinetics (Fig. 3) and were not inhibited at lower pH_o . The half-maximal H^+ concentration ($K_{0.5}^{\text{H}}$) was $\approx 1\text{ }\mu\text{M}$, i.e. pH_o

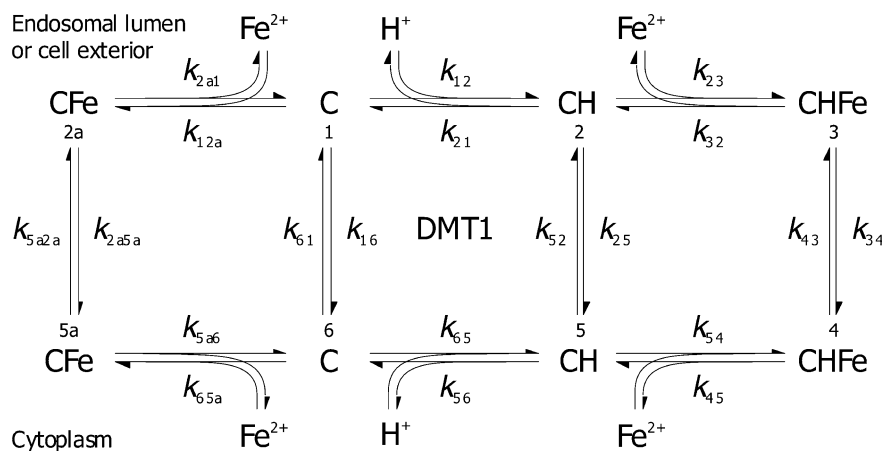


Fig. 8 Mechanisms of DMT1. We propose an eight-state model for the binding and transport of H^+ and Fe^{2+} by rat DMT1. Each reaction step $x \rightarrow y$ is described by its rate constant k_{xy} . We anticipate that at least k_{16} , k_{61} , k_{12} , and k_{21} (rates describing reorientation of the empty, charged carrier and binding/dissociation of H^+) will contain voltage-dependent terms, and that rate constants describing binding/dissociation steps are modified by

extracellular or intracellular ligand (H^+ , Fe^{2+}) concentrations. This model can be tested, and rate constants estimated, by computer simulation. In addition to $\text{H}^+/\text{Fe}^{2+}$ cotransport (step $3 \rightarrow 4$), we observed under certain conditions a H^+ leak or uniport (step $2 \rightarrow 5$) and facilitative (H^+ -uncoupled) Fe^{2+} transport (step $2a \rightarrow 5a$)

6.0, which closely matches the extracellular pH within the acid microclimate of the mammalian small intestine brush border. Mucosal surface pH in the jejunum was measured at 6.0–6.2 in the rat in vivo [37, 47, 48] and in control human subjects in situ [38, 46]. Therefore, we anticipate that intestinal absorption of iron will be modulated by small pH changes in the mucosal surface acid microclimate.

Worthington et al. [57] questioned our conclusion [19] that the H^+ electrochemical potential gradient drives Fe^{2+} transport via a saturable cotransport mechanism in DMT1. Finding that Fe^{2+} transport in COS-7 cells and Caco-2 cells expressing human DMT1 was nonsaturable and exhibited an optimum at pH 6.75, these authors concluded that the Fe^{2+} -evoked currents we observed in oocytes reflect only a H^+ current and not Fe^{2+} transport per se, and that Fe^{2+} and H^+ are uncoupled. Whereas it is known that the inward current exceeds that expected for strict stoichiometric $\text{H}^+/\text{Fe}^{2+}$ cotransport in oocytes expressing DMT1 [7, 59], we demonstrate here that the pH-dependence of $^{55}\text{Fe}^{2+}$ uptake is identical to that of the Fe^{2+} -evoked currents in oocytes expressing rat DMT1 (see Fig. 2c, c.f. Fig. 7e). The inhibition of Fe^{2+} uptake reported in COS-7 or Caco-2 cells at low pH_o [57] may have resulted from a loss of integrity of the cell-culture monolayers when exposed to low pH_o over the 2 h incubation period. In a separate study [51] using *fully differentiated* Caco-2 cells expressing human DMT1, $^{55}\text{Fe}^{2+}$ uptake (1 h) displayed a pH dependence similar to that observed by us for DMT1-expressing oocytes. Likewise in CHO cells expressing DMT1 (Nramp2), Fe^{2+} or Mn^{2+} transport (measured by fluorescence quenching of metal-ion-sensitive dyes) was stimulated at low pH_o , and the existence of an optimal pH_o was not apparent within the pH_o range 7.0–5.0 [14, 29].

Mechanisms of DMT1

From our present biophysical data, we have arrived at an eight-state model (Fig. 8) to describe the mechanisms of DMT1. We conclude that DMT1 mediates both simultaneous H^+ -coupled Fe^{2+} transport and thermodynamically uncoupled fluxes of H^+ or Fe^{2+} depending on prevailing conditions. Analysis of the partial activities retained by H272A-DMT1, for which Fe^{2+} transport is uncoupled from the H^+ flux, demonstrated that the DMT1 protein possesses the machinery to catalyze facilitative Fe^{2+} transport without H^+ coupling. Our evidence for H^+ -uncoupled Fe^{2+} transport is also derived from the observations that (i) a fraction of the $^{55}\text{Fe}^{2+}$ uptake and Fe^{2+} -evoked currents in DMT1-expressing oocytes persisted at neutral pH_o , (Figs. 2c, 7e) and (ii) mathematical fits of saturation kinetics data at $\text{pH}_o > 6.1$ support competition between Fe^{2+} and H^+ for the empty carrier (Fig. 3a, e). Our data are not explained by a *six-state consecutive transport* model (i.e. one in which only one of the two ligands is translocated in a single cycle), since there is evidence of competition between Fe^{2+} and H^+ (and their subsequent uniport) only when $[\text{H}^+]_o$ is very low. Instead, our data for $K_{0.5}^{\text{H}}$ (Fig. 3b) and $K_{0.5}^{\text{Fe}}$ at $\text{pH}_o < 6.1$ (Fig. 3e) are consistent with a *simultaneous* $\text{H}^+/\text{Fe}^{2+}$ cotransport model [25, 49].

Why are alternative six-state simultaneous transport models insufficient to explain our data? We first considered a *six-state ordered-binding simultaneous transport* model (i.e. excluding states 2a and 5a from our model, Fig. 8). The observation of H^+ -sensitive presteady-state currents only in the absence of metal ion is consistent with H^+ being the first ligand to bind to DMT1. Since Fe^{2+} inhibits the H^+ leak mediated by H272A-DMT1, in such a model we should expect Fe^{2+} binding to lock

the mutant transporter in a nontransporting state (state 3, Fig. 8). This would be analogous with the way in which phlorizin inhibits the Na^+ leak in the Na^+ /glucose cotransporters by binding to the sugar-binding site without itself being transported [9, 31, 35, 43, 44]. However, Fe^{2+} binding to H272A-DMT1 instead resulted in pH_0 -independent Fe^{2+} transport (Fig. 5).

Can our data satisfy a six-state, simultaneous transport model in which ligand binding is *random*? The dependence of $I_{\text{max}}^{\text{Fe}}$ on $[\text{H}^+]_0$ (Fig. 3f) appears to support such a mechanism, and the pH -independence of the H272A-DMT1-mediated $^{55}\text{Fe}^{2+}$ uptake (Fig. 5) might be explained if the impact of the H272A mutation were to markedly increase affinity for H^+ such that $0.1 \mu\text{M}$ H^+ (pH_0 7.0) were saturating. However, in a *random-binding simultaneous transport* mechanism, addition of Fe^{2+} to H272A-DMT1 should be expected to accelerate the H^+ flux and current. Instead, H272A-mediated Fe^{2+} transport was associated with a significant inhibition of H^+ influx (Fig. 4c) and overall current (Fig. 6a, d), indicating that H^+ and Fe^{2+} compete for the empty mutant transporter and are translocated independently (i.e. H272A-DMT1 is described by the model in Fig. 8, excluding states 3 and 4).

A recent observation in the literature lends strong support to our conclusion that DMT1 mediates H^+ -uncoupled facilitative metal-ion transport at higher pH_0 . Xu and coworkers measured the reversal potential (V_r or E_{rev}) of the Mn^{2+} -evoked currents in DMT1-transfected CHO cells [59]. The slope of V_r versus pH_0 was close to the predicted Nernst potential for a H^+ selective electrode at $\text{pH}_0 < 5.8$. However, V_r varied little at $\text{pH}_0 > 5.8$, indicating an increased permeability for Mn^{2+} relative to H^+ at higher pH_0 .

Future studies may be directed towards further testing our model (Fig. 8), deriving specific rate constants with the aid of computer simulation, and defining the rate-determining steps. The maximal turnover rate for wtDMT1 (or H267A-DMT1) was $21\text{--}23 \text{ s}^{-1}$ at -150 mV (Table 2) and much slower at depolarized V_m . The inverse of this rate provides us with the minimum time required to complete one transport cycle, $43\text{--}48 \text{ ms}$. Since most of the presteady-state charge transfer is complete within this time (τ_{max} was 32 ms at $+61 \text{ mV}$), we conclude that transporter reorientation (step $6 \rightarrow 1$) and H^+ binding (step $1 \rightarrow 2$) are not rate-limiting at any V_m . Since the $K_{0.5}^{\text{Fe}}$ (which reflects Fe^{2+} binding and transport) in wtDMT1 significantly exceeded the K_i^{Fe} (reflecting Fe^{2+} binding) in H272A-DMT1 (Table 2), we also conclude that Fe^{2+} binding (step $2 \rightarrow 3$) is not rate limiting, at least at physiological V_m (-50 to -70 mV).

Transport of Zn^{2+} by DMT1

The wtDMT1 exhibited a marked preference for Fe^{2+} over Zn^{2+} , resulting from both a lower maximal transport and a reduced apparent affinity for Zn^{2+} compared

with Fe^{2+} . This preference was abolished by the H272A mutation, which lowered $I_{\text{max}}^{\text{Fe}}$ and increased $K_{0.5}^{\text{Fe}}$. These kinetic data provide further evidence that His-272 plays a structural role in the DMT1 H^+ -to- Fe^{2+} coupling mechanism. His-272 also appears to be involved in transducing the effect of H^+ binding (via a conformational change) to increase the affinity with which DMT1 binds Fe^{2+} . On the basis of our H272A data, H^+ binding may not alter the affinity of DMT1 to bind Zn^{2+} . Evidence that Zn^{2+} transport is not limited to the facilitative metal-ion transport route comes from the observations that Zn^{2+} transport was (i) pH -dependent and (ii) associated with intracellular acidification (Fig. 7e, f). Although, Zn^{2+} is poorly transported relative to Fe^{2+} , we have shown previously that Zn^{2+} is one of several divalent metal ions that evoke currents of a similar magnitude to the Fe^{2+} -evoked currents in oocytes expressing wtDMT1 at -50 mV [19]. Therefore, DMT1-mediated Zn^{2+} transport may be associated with significant slippage of H^+ , or Zn^{2+} may induce in DMT1-expressing oocytes a conductance for another ion.

Conclusions

We have identified His-272 as critical in the coupling of metal-ion transport to the H^+ flux through DMT1. Histidyl residues may be titratable within the physiological pH range. Since mutating His-272 to an alanyl or arginyl residue disrupted coupling, transient protonation of His-272 may be a requirement for the H^+ -coupling of DMT1.

DMT1 is responsible both for apical membrane Fe^{2+} transport in epithelial systems and for its cellular uptake via TfR-associated endocytosis, as in erythroid precursors. The acid microclimate of the intestinal brush border and the endosomal acidification in erythroid cells provide transmembrane H^+ gradients that will allow DMT1 to be highly concentrative. However, our study reveals for the first time an uncoupled Fe^{2+} transport mode in DMT1, with Fe^{2+} transport driven by the electrochemical gradient for Fe^{2+} alone. Whereas H^+ -coupling (and the H^+ -dependent increase in affinity for Fe^{2+}) in *acidified* endosomes will ensure that DMT1 is an effective scavenger of endosomal Fe^{2+} , DMT1-mediated facilitative Fe^{2+} transport may permit mobilization of Fe^{2+} from endosome to cytosol even before significant luminal acidification. Notably, in erythroid precursors, Fe^{3+} may be liberated from the transferrin-TfR complex following only a small drop in endosomal pH [40].

Our identification of facilitative Fe^{2+} transport at neutral pH raises the possibility that DMT1 may also be operational at the *plasma* membrane of cells facing a neutral- pH environment. Whether this is of physiological relevance in various cell types will have to be determined, but it is likely to be of significant importance in iron overload conditions. For example, substantial increases in nontransferrin-bound plasma iron (NTBI) are common in the hemoglobinopathies and disorders

involving defective erythropoiesis, e.g. thalassemia (compounded by transfusional iron overload), and in hereditary hemochromatosis [8, 17, 22, 42]. Much of this NTBI will be cleared by the liver after it is reduced to Fe^{2+} [54, 58], and strong evidence exists for the presence of ferrireductase activity at the cell surface of hepatocytes [39] and other cell types [24, 26]. Notably, DMT1 is upregulated at the plasma membrane of hepatocytes in iron overload [53] and is also expressed in the heart [19, 23, 27], a major site of iron toxicity in overload [20]. Thus, H^+ -uncoupled Fe^{2+} transport mediated by DMT1 expressed at the plasma membrane can account for the hepatic accumulation of NTBI and directly contribute to the etiology of hepatic and cardiac toxicity in iron overload disorders.

Acknowledgments We are grateful to Hitomi Takanaga and Jonathan Sabbagh for their help in the laboratory, and to William A. Stein for advice regarding mathematical fitting. This study was supported by NIH grants R01-DK057782 (to M.A.H.) and R01-DK056218 (to M.F.R.), and a pilot/feasibility award (to B.M.) from the Harvard Digestive Diseases Center, funded by NIH center grant P30-DK034854.

References

- Aslamkhan AG, Aslamkhan A, Ahearn GA (2002) Preparation of metal ion buffers for biological experimentation: a methods approach with emphasis on iron and zinc. *J Exp Biol* 292:507–522
- Bannon DI, Abounader R, Lees PS, Bressler JP (2003) Effect of DMT1 knockdown on iron, cadmium, and lead uptake in Caco-2 cells. *Am J Physiol Cell Physiol* 284:C44–C50
- Becker HM, Bröer S, Deitmer JW (2004) Facilitated lactate transport by MCT1 when coexpressed with the sodium bicarbonate cotransporter (NBC) in *Xenopus* oocytes. *Biophys J* 86:235–247
- Canonne-Hergaux F, Gros P (2002) Expression of the iron transporter DMT1 in kidney from normal and anemic *mk* mice. *Kidney Int* 62:147–156
- Canonne-Hergaux F, Gruenheid S, Ponka P, Gros P (1999) Cellular and subcellular localization of the Nramp2 iron transporter in the intestinal brush border and regulation by dietary iron. *Blood* 93:4406–4417
- Canonne-Hergaux F, Zhang A-S, Ponka P, Gros P (2001) Characterization of the iron transporter DMT1 (NRAMP2/DCT1) in red blood cells of normal and anemic *mk/mk* mice. *Blood* 98:3823–3830
- Chen X-Z, Peng J-B, Cohen A, Nelson H, Nelson N, Hediger MA (1999) Yeast SMF1 mediates H^+ -coupled iron uptake with concomitant uncoupled cation currents. *J Biol Chem* 274:35089–35094
- de Valk B, Addicks MA, Gosriwatana I, Lu S, Hider RC, Marx JJ (2000) Non-transferrin-bound iron is present in serum of hereditary haemochromatosis heterozygotes. *Eur J Clin Invest* 30:248–251
- Diez-Sampedro A, Lostao MP, Wright EM, Hirayama BA (2000) Glycoside binding and translocation in Na^+ -dependent glucose cotransporters: comparison of SGLT1 and SGLT3. *J Membr Biol* 176:111–117
- Dinour D, Chang M-H, Satoh J, Smith BL, Angle N, Knecht A, Serban I, Holtzman EJ, Romero MF (2004) A novel missense mutation in the sodium bicarbonate cotransporter (NBCe1/SLC4A4) causes proximal tubular acidosis and glaucoma through ion transport defects. *J Biol Chem* 279:52238–52246
- Fischer BE, Haring UK, Tribolet R, Sigel H (1979) Metal ion/buffer interactions: stability of binary and ternary complexes containing 2-amino-2(hydroxymethyl)-1,3-propanediol (Tris) and adenosine 5'-triphosphate (ATP). *Eur J Biochem* 94:523–530
- Fleming MD, Romano MA, Su MA, Garrick LM, Garrick MD, Andrews NC (1998) *Nramp2* is mutated in the anemic Belgrade (*b*) rat: evidence of a role for Nramp2 in endosomal iron transport. *Proc Natl Acad Sci USA* 95:1148–1153
- Fleming MD, Trenor CC, Su MA, Foernzler D, Beier DR, Dietrich WF, Andrews NC (1997) Microcytic anaemia mice have a mutation in *Nramp2*, a candidate iron transporter gene. *Nat Genet* 16:383–386
- Forbes JR, Gros P (2003) Iron, manganese, and cobalt transport by Nramp1 (Slc11a1) and Nramp2 (Slc11a2) expressed at the plasma membrane. *Blood* 102:1884–1892
- Garrick LM, Dolan KG, Romano MA, Garrick MD (1999) Non-transferrin-bound iron uptake in Belgrade and normal rat erythroid cells. *J Cell Physiol* 178:349–358
- Garrick MD, Dolan KG, Horbinski C, Ghio AJ, Higgins D, Porubcin M, Moore EG, Hainsworth LN, Umbreit JN, Conrad ME, Feng L, Lis A, Roth JA, Singleton S, Garrick LM (2003) DMT1: a mammalian transporter for multiple metals. *Bio-metals* 16:41–54
- Grootveld M, Bell JD, Halliwell B, Aruoma OI, Bomford A, Sadler PJ (1989) Non-transferrin-bound iron in plasma or serum from patients with idiopathic hemochromatosis. Characterization by high performance liquid chromatography and nuclear magnetic resonance spectroscopy. *J Biol Chem* 264:4417–4422
- Gruenheid S, Canonne-Hergaux F, Gauthier S, Hackam DJ, Grinstein S, Gros P (1999) The iron transport protein NRAMP2 is an integral membrane glycoprotein that colocalizes with transferrin in recycling endosomes. *J Exp Med* 189:831–841
- Gunshin H, Mackenzie B, Berger UV, Gunshin Y, Romero MF, Boron WF, Nussberger S, Gollan JL, Hediger MA (1997) Cloning and characterization of a proton-coupled mammalian metal-ion transporter. *Nature* 388:482–488
- Harrison SA, Bacon BR (2003) Hereditary hemochromatosis: update for 2003. *J Hepatol* 38:S14–S23
- Hazama A, Loo DDF, Wright EM (1997) Presteady-state currents of the rabbit Na^+ /glucose cotransporter (SGLT1). *J Membr Biol* 155:175–186
- Hershko C, Graham G, Bates GW, Rachmilewitz EA (1978) Non-specific serum iron in thalassaemia: an abnormal serum iron fraction of potential toxicity. *Br J Haematol* 40:255–263
- Hubert N, Hentze MW (2002) Previously uncharacterized isoforms of divalent metal transporter (DMT)-1: implications for regulation and cellular function. *Proc Natl Acad Sci USA* 99:12345–12350
- Inman RS, Coughlan MM, Wessling-Resnick M (1994) Extracellular ferrireductase activity of K562 cells is coupled to transferrin-independent iron transport. *Biochemistry* 33:11850–11857
- Jauch P, Läuger P (1986) Electrogenic properties of the sodium-alanine cotransporter in pancreatic acinar cells: II. Comparison with transport models. *J Membr Biol* 94:117–127
- Jordan I, Kaplan J (1994) The mammalian transferrin-independent iron transport system may involve a surface ferrireductase activity. *Biochem J* 302:875–879
- Ke Y, Chen YY, Chang YZ, Duan XL, Ho KP, Jiang DH, Wang K, Qian ZM (2003) Post-transcriptional expression of DMT1 in the heart of rat. *J Cell Physiol* 196:124–130
- Klamo EM, Drew ME, Landfear SM, Kavanaugh MP (1996) Kinetics and stoichiometry of a proton/*myo*-inositol cotransporter. *J Biol Chem* 271:14937–14943
- Lam-Yuk-Tseung S, Govoni G, Gros P (2003) Iron transport by NRAMP2/DMT1: pH regulation of transport by two histidines in transmembrane domain 6. *Blood* 101:3699–3707
- Loo DDF, Hazama A, Supplisson S, Turk E, Wright EM (1993) Relaxation kinetics of the Na^+ /glucose cotransporter. *Proc Natl Acad Sci USA* 90:5767–5771

31. Lostao MP, Hirayama BA, Loo DDF, Wright EM (1994) Phenylglucosides and the Na^+ /glucose cotransporter (SGLT1): analysis of interactions. *J Membr Biol* 142:161–170
32. Mackenzie B (1999) Selected techniques in membrane transport. In: Van Winkle LJ (ed) *Biomembrane transport*. Academic Press, San Diego, pp 327–342
33. Mackenzie B, Hediger MA (2004) SLC11 family of H^+ -coupled metal-ion transporters NRAMP1 and DMT1. *Pflügers Arch Eur J Physiol* 447:571–579
34. Mackenzie B, Loo DDF, Fei YJ, Liu W, Ganapathy V, Leibach FH, Wright EM (1996) Mechanisms of the human intestinal H^+ -coupled oligopeptide transporter hPEPT1. *J Biol Chem* 271:5430–5437
35. Mackenzie B, Loo DDF, Panayotova-Heiermann M, Wright EM (1996) Biophysical characteristics of the pig kidney Na^+ /glucose cotransporter SGLT2 reveal a common mechanism for SGLT1 and SGLT2. *J Biol Chem* 271:32678–32683
36. Mackenzie B, Schäfer MKH, Erickson JD, Hediger MA, Weihe E, Varoqui H (2003) Functional properties and cellular distribution of the System A glutamine transporter SNAT1 support specialized roles in central neurons. *J Biol Chem* 278:23720–23730
37. McEwan GTA, Daniel H, Fett C, Burgess MN, Lucas ML (1988) The effect of *Escherichia coli* STa enterotoxin and other secretagogues on mucosal surface pH of rat small intestine in vivo. *Proc R Soc Lond B* 234:219–237
38. McEwan GTA, Lucas ML, Mathan VI (1990) A combined TDDA-PVC pH and reference electrode for use in the upper small intestine. *J Med Eng Tech* 14:16–20
39. Moridani MY, O'Brien PJ (2001) Iron complexes of deferiprone and dietary plant catechols as cytoprotective superoxide radical scavengers (I). *Biochem Pharmacol* 62:1579–1585
40. Núñez M-T, Gaete V, Watkins JA, Glass J (1990) Mobilization of iron from endocytic vesicles. The effects of acidification and reduction. *J Biol Chem* 265:6688–6692
41. Núñez M-T, Gaete V, Watkins JA, Glass J (1990) Mobilization of iron from endocytic vesicles. The effects of acidification and reduction. *J Biol Chem* 265:6688–6692
42. Olivieri NF (2002) Transfusional iron overload. In: Templeton DM (ed) *Molecular and cellular iron transport*. Marcel-Dekker, New York, pp 725–747
43. Parent L, Supplisson S, Loo DDF, Wright EM (1992) Electrogenic properties of the cloned Na^+ /glucose cotransporter: I. Voltage-clamp studies. *J Membr Biol* 125:49–62
44. Parent L, Supplisson S, Loo DDF, Wright EM (1992) Electrogenic properties of the cloned Na^+ /glucose cotransporter: II. A transport model under nonrapid equilibrium conditions. *J Membr Biol* 125:63–79
45. Picard V, Govoni G, Jabado N, Gros P (2000) Nramp 2 (DCT1/DMT1) expressed at the plasma membrane transports iron and other divalent cations into a calcein-accessible cytoplasmic pool. *J Biol Chem* 275:35738–35745
46. Rawlings JM, Lucas ML, Russell RI (1987) Measurement of jejunal surface pH in situ by plastic pH electrode in patients with coeliac disease. *Scand J Gastroenterol* 22:377–384
47. Said HM, Tipton W, Nylander W, Urban E (1987) Effect of small bowel resection on the intestinal surface acid microclimate in the rat. *Digestion* 38:221–225
48. Shimada T, Hoshi T (1988) Na^+ -dependent elevation of the acidic cell surface pH (microclimate pH) of rat jejunal villus cells induced by cyclic nucleotides and phorbol ester: possible mediators of the regulation of the Na^+/H^+ antiporter. *Biochim Biophys Acta* 937:328–334
49. Stein WD (1986) *Transport and diffusion across cell membranes*. Academic Press, Orlando
50. Su MA, Trenor CC, Fleming JC, Fleming MD, Andrews NC (1998) The G185R mutation disrupts function of the iron transporter Nramp2. *Blood* 92:2157–2163
51. Tandy S, Williams M, Leggett A, Lopez-Jimenez M, Dedes M, Ramesh B, Srai SK, Sharp P (2000) Nramp2 expression is associated with pH-dependent iron uptake across the apical membrane of human intestinal Caco-2 cells. *J Biol Chem* 275:1023–1029
52. Touret N, Furuya W, Forbes J, Gros P, Grinstein S (2003) Dynamic traffic through the recycling compartment couples the metal transporter Nramp2 (DMT1) with the transferrin receptor. *J Biol Chem* 278:25548–25557
53. Trinder D, Oates PS, Thomas C, Sadleir J, Morgan EH (2000) Localisation of divalent metal transporter 1 (DMT1) to the microvillus membrane of rat duodenal enterocytes in iron deficiency, but to hepatocytes in iron overload. *Gut* 46:270–276
54. Trinder D, Morgan E (1998) Mechanisms of ferric citrate uptake by human hepatoma cells. *Am J Physiol Gastrointest Liver Physiol* 275:G279–G286
55. Wadiche JI, Arriza JL, Amara SG, Kavanaugh MP (1995) Kinetics of a human glutamate transporter. *Neuron* 14:1019–1027
56. Wareing M, Ferguson CJ, Green R, Riccardi D, Smith CP (2000) In vivo characterization of renal iron transport in the anaesthetized rat. *J Physiol* 524:581–586
57. Worthington MT, Browne L, Battle EH, Luo RQ (2000) Functional properties of transfected human DMT1 iron transporter. *Am J Physiol Gastrointest Liver Physiol* 279:G1265–G1273
58. Wright TL, Brissot P, Ma W-L, Weisiger RA (1986) Characterization of non-transferrin-bound iron clearance by rat liver. *J Biol Chem* 261:10909–10914
59. Xu H, Jin J, DeFelice LJ, Andrews NC, Clapham DE (2004) A spontaneous, recurrent mutation in divalent metal transporter-1 exposes a calcium entry pathway. *PLoS Biol* 2:E50
60. Yu Q, Kandegedara A, Xu Y, Rorabacher DB (1997) Avoiding interferences from Good's buffers: A contiguous series of noncomplexing tertiary amine buffers covering the entire range of pH 3–11. *Anal Biochem* 253:50–56
61. Zampighi GA, Kreman M, Boorer KJ, Loo DDF, Bezanilla F, Chandy G, Hall JE, Wright EM (1995) A method for determining the unitary functional capacity of cloned channels and transporters expressed in *Xenopus laevis* oocytes. *J Membr Biol* 148:65–78